Small Cell Networks with Fractal Coverage Characteristics

Xiaohu Ge, *Senior Member, IEEE*, Xiaotong Tian, Yehong Qiu,
Guoqiang Mao, *Senior Member, IEEE*, Tao Han, *Member, IEEE*

***Abstract*—To meet massive wireless traffic demand in the future fifth generation (5G) cellular networks, small cell networks are emerging as an attractive solution for 5G network deployments. The cellular coverage characteristic is a key issue for the deployment of small cell networks. Considering the anisotropic path loss in wireless channels of real cellular scenarios, in this paper the fractal coverage characteristic is first used to evaluate the performance of small cell networks. Moreover, the coverage probability, average achievable rate and the area spectral efficiency are derived for fractal small cell networks. Compared with the average achievable rate and area spectral efficiency with isotropic path loss models, the average achievable rate and area spectral efficiency with anisotropic path loss models has been underestimated in fractal small cell networks. Considering the impact of the anisotropic path loss on wireless channels, most of performances of wireless cellular networks need to be re-evaluated. This paper provides a tractable method to investigate the performance of small cell networks with fractal coverage characteristics.**

***Index Terms*—Small cell, wireless fractal coverage model, coverage probability, area spectral efficiency, anisotropic path loss.**

I. Introduction

MOTIVATED by new applications, *e.g.,* virtual reality and augmented reality applications, the wireless traffic will increase more than 1000 times for 5G cellular networks in the next decade [1], [2]. As one of the potential solutions, the idea of providing small cell deployments has proven to be an attractive solution to meet the 1000 times capacity crunch [3]–[5], while bringing additional energy efficiency (EE) to the system as well. Different from macro cells, small cells with lower transmission power are mostly deployed in high traffic demand areas, e.g., urban scenarios. However, due to the irregularly distributed buildings, non-uniformly distributed vegetation and changing weather in those areas, the wireless propagation environment is quite changeable and complex, which results in the irregular wireless coverage of small cell and influences the performance of small cell networks. The measurement results in [6] indicated that the irregular cellular coverage boundary in actual wireless communication environments has the statistical fractal characteristic in angular scales. Hence, to optimize the deployment of small cell networks, the complexity of wireless propagation environments and wireless coverage characteristics need to be considered for performance evaluation of small cell networks. However, considering the complexity of wireless propagation environment, it is a great challenge to investigate the performance of small cell networks with wireless fractal coverage characteristics.

The authors would like to acknowledge the support from the Hubei Provincial Science and Technology Department under Grant 2016AHB006, the China International Joint Research Center of Green Communications and Networking under Grant 2015B01008 and the National Natural Science Foundation of China under Grant 61471180. This research is partially supported by the EU FP7-PEOPLE-IRSES, the project acronym CROWN under Grant 610524, the project acronym EXCITING under Grant 723227. *(Corresponding author: T. Han.)*

X. Ge, X. Tian, Y. Qiu and T. Han are with the School of Electronic Information and Communications, Huazhong University of Science and Technology, Wuhan 430074, Hubei, China (email: {xhge, xiaotong_tian, yehong_qiu, hantao}@mail.hust.edu.cn).

G. Mao is with University of Technology Sydney and National ICT Australia, Sydney, Australia (email: g.mao@ieee.org).

A. Related Work

Most of existing studies involving with small cell networks have been based on the assumption of seamless coverage scenarios, such as the regular hexagon cellular coverage model and Poisson-Voronoi tessellation (PVT) cellular networks [7]–[12]. In conventional performance analysis of cellular networks, the regular hexagon cellular coverage model has been widely adopted in [7], [8]. Based on the regular hexagon cellular coverage model, a pilot reuse scheme was proposed to analyze the lower bound of uplinks in a massive MIMO wireless communication system [7]. Utilizing the fractional frequency reuse scheme, the regular hexagon cellular coverage region was divided into the center region and the edge region to investigate the coverage probability and the available rate for cellular networks [8]. Although the regular hexagon cellular coverage model can easily build a cellular network for realizing the seamless and non-overlap coverage [9], the impact of the density of base stations (BSs) on the performance cellular networks is ignored. However, the locations of BSs usually are random and the coverage areas of BSs are often irregular in real cellular scenarios [10]. To overcome these shortcomings, the locations of BSs have been assumed to be governed by Poisson point processes and cellular coverage regions have been partitioned by a Delaunay triangulation method to establish seamless random cellular networks [11], [12]. Based on Poisson-Voronoi tessellation (PVT) cellular networks, a

tractable approach was proposed to analyze the coverage probability and available rates in random cellular networks [11]. Considering the user traffic load in cellular regions, a Markov chain based wireless channel access model was used to evaluate the spatial spectral and energy efficiency of PVT random cellular networks [12]. In general, the two cellular coverage models mentioned above are used for seamless networks and both define the cell coverage boundary by geometric partitioning. But irregular distribution buildings and shelters in actual wireless communication environments result in the complex attenuation of wireless signals and the irregular cell coverage boundary, which make some users not) associate with the cellular networks successfully. Hence, the "leakage cover" phenomenon is inevitable in wireless cellular networks.

The path loss is one of the key components for complex wireless transmission channels. Most of the existing studies involving small cell networks have been based on the assumptions of conventional path loss models [13], [14]. The conventional path loss fading models imply that the wireless signal power decays like a power-law over the propagation distance and the decay rates called path loss coefficients are the same in different propagation directions, which is called isotropic path loss model in this paper. Utilizing a non-uniform deployment scheme with isotropic path loss model, the downlink coverage and throughput performance of small cell networks were investigated in [14]. When small cells are ultra-densely deployed in urban regions, the non-line-of-sight (NLoS) and line-of-sight (LoS) wireless transmissions have been simultaneously existed in small cell networks. In these cases, conventional path loss models, *i.e.,* isotropic path loss models, have been indicated to be not suitable for small cell networks [15]. A stochastic path loss model incorporating both LoS and NLoS wireless transmissions was introduced to investigate their impact on the performance of dense small cell networks [16]. A stochastic geometry framework was proposed to study the coverage probability, the spectral efficiency and the area spectral efficiency of dense small cell networks where the path loss model includes both LoS and NLoS components [17]. Multi-slope path loss models, where different distance ranges are subject to different path loss exponents, were proposed to analyze the throughput and the coverage probability of cellular networks [18].

In above studies, the differentiation of path loss coefficients has been limited in different distance ranges. However, buildings and obstacles are distributed irregularly in urban environments and electromagnetic waves in different directions experience different path loss considering different diffraction and scattering effects in different propagation directions, which conduce to the non-seamless coverage and irregular coverage boundary in real cellular scenarios. The path loss models, *i.e.,* the path loss coefficients are different not only in different propagation distance ranges, but also in different propagation directions even with the same distance range in real cellular scenarios. Therefore, the path loss models are anisotropic in real cellular scenarios. Small cells are mainly deployed in urban environment to offload the wireless traffic from macro cell BSs [19], since it is an inevitable challenge to investigate the impact of anisotropic path loss on the performance of small cell networks.

B. Contributions and Organizations

Based on our measurement results in [6] and related research work mentioned above, in this paper, the fractal characteristic of cellular coverage and anisotropic path loss model are first utilized to investigate the performance of small cell networks. The main contributions of this paper are summarized as follows:

1) Compared with conventional seamless coverage scenarios, a stochastic geometry small cell scenario with irregular wireless fractal coverage is proposed to analyze the coverage probability, the average achievable rate and area spectral efficiency in small cell networks. The wireless fractal coverage characteristic is able to capture the anisotropy of path loss in realistic propagation environments in small cell networks.
2) Based on the wireless fractal coverage characteristic, the coverage probability, the average achievable rate and the area spectral efficiency are derived for the performance analysis of small cell networks. Moreover, the lower bound of average achievable rate is derived for a typical user in fractal small cell networks.

The main observations of this paper are list as follows:

1) Compared with the coverage probability with isotropic path loss models in small cell networks, analytical and Monto-Carlo simulation results indicate that the coverage probability with anisotropic path loss models has been overestimated in low signal-to-interference ratio (SIR) regimes and has been underestimated in high SIR regimes.
2) Compared with the average achievable rate and area spectral efficiency with isotropic path loss models, the average achievable rate and area spectral efficiency with anisotropic path loss models have been underestimated in fractal small cell networks.

The rest of the paper is organized as follows. Section II describes the system model. In Section III, the coverage probability, the average achievable rate and the area spectral efficiency have been derived for small cell networks based on wireless fractal coverage characteristics. Furthermore, the performance analysis of fractal coverage small cell networks with anisotropic path loss has been simulated and compared with the performance of fractal small cell networks with isotropic path loss in Section IV. Finally, Section V concludes this paper.

II. System Model

A. Fractal Foundation

Fractals are complex geometric features exhibiting self-similar properties in that small details of its structure viewed at any scale repeat elements of the overall pattern. As mathematical equations, fractals are usually nowhere differentiable. An infinite fractal curve can be conceived of as winding through space differently from an ordinary line, still being a 1-dimensional line yet having a fractal dimension indicating it also resembles a surface [20]. A fractal dimension is an index for characterizing fractal patterns or sets by quantifying their complexity as a ratio of the change in detail to the change in scale. The quantization of a fractal dimension is typically estimated by the value of the Hurst parameter. Three typical statistical estimators, that is, the periodogram method, the rescaled adjusted range statistic (R/S) method, and the variance-time analysis method, are utilized to estimate the value of the Hurst parameter for real worlds [21]. Our measured results indicated that the irregular cellular coverage boundary in actual wireless communication environments has the fractal characteristic in statistics [6].

B. Network Model

In this paper our studies focus on downlinks of small cell networks. Assume that small cell BSs (SBSs) are located randomly in an infinite plane. We consider that the locations of user/SBS are modeled as a Poisson cluster process (PCP), with the parent point process, i.e., the locations of SBSs modeled as a Poisson point process (PPP) denoted by Φ_B having density λ_B, and the daughter point processes are independent and identically distributed (i.i.d.), i.e., the locations of users modeled as an independent Bernoulli process Φ_u with density λ_u. Every SBS is assumed to be equipped with N_t transmission antennas and have the same transmission power p_t(W). Every small cell is associated with one SBS. Without loss of generality, a fractal small cell C_0, where the SBS SBS_0 is associated, is selected to evaluate the performance of small cell networks. Every user is equipped with single receive antenna. The number of users served by each SBS in a given resource block is N_r and $N_r \leq N_t$.

Based on our measured results [6], the coverage boundary of cellular scenario has the fractal characteristic, *i.e.,* the distance distribution between the SBS and the coverage boundary that presents the fractal characteristic in the angle domain, which is defined as fractal small cells in this paper and the fractal characteristic is caused by the anisotropic of path loss in real propagation environments. The system model is illustrated in Fig. 1, where the SBS SBS_0 is marked as blue and the blue real line is the coverage boundary of fractal small cells.

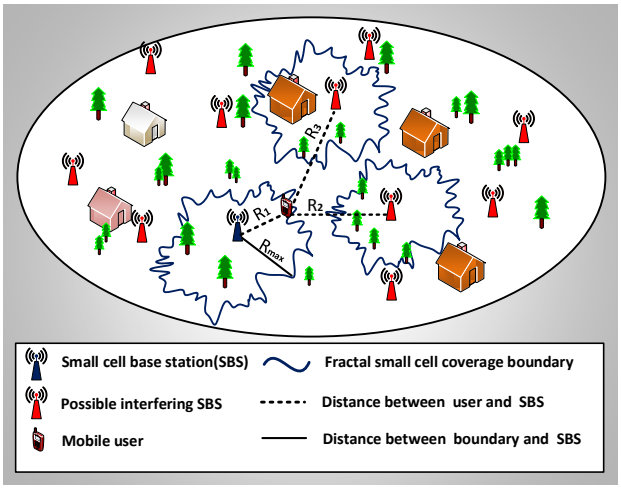

Fig. 1. System model

The orthogonal frequency division multiplexing (OFDM) technique with frequency reuse factor δ is assumed to be adopted for the access process in small cell networks and every subcarrier frequency is only serviced for one user in a time slot. Hence, there is no intra-cell interference in a fractal small cell. Active users are interfered by the interference from adjacent fractal small cells using the same transmission frequency.

Obviously, different from the traditional hexagonal and PVT cellular networks which split the two-dimensional plane into multiple regular triangles, squares, or regular hexagons that seamlessly cover the service region without overlaps, the fractal small cell network proposed in this paper is a seam cover network, which means that a user located outside the coverage boundary is omitted in cellular networks.

C. Path Loss Model

Without loss of generality, the traditional path loss model is denoted by $l = r^{-\beta}$, where β is the path loss coefficient and assumed to be the same in all propagation directions, *i.e.,* the isotropic path loss model. However, the propagation of electromagnetic waves in objects is complicated and is affected by various factors including the carrier frequency, the height of antennas, the nature of the terrain, the urbanization, changes in atmospheric and weather environment, the speed of mobile users, changes in foliage conditions, the surrounding buildings, obstacle distributions, scatterers, and so on [22]. Especially, surrounding buildings and scatterers are distributed irregularly in urban environments which is showed in Fig. 1. As a consequence, the path loss of wireless signals is different not only in different propagation distance ranges, but also obviously in different propagation directions because many of those factors are random in natural urban environments. However, the traditional path loss *i.e.,* the

This article has been accepted for publication in a future issue of this journal, but has not been fully edited. Content may change prior to final publication. Citation information: DOI 10.1109/TCOMM.2018.2849391, IEEE Transactions on Communications

isotropic path loss model in a cellular coverage has been assumed to be same in different directions without considering the anisotropic of path loss in urban environments.

The distance between the small cell BS and the coverage boundary is denoted as $R_{\max}$, the transmission power of small cell BS is configured as p_t, the farthest locations of the cell coverage area are denoted as the wireless cellular coverage boundary points, where the average received wireless signal power is equal to the minimum threshold $P_{\min}$(W). Based on the results in [18], the path loss coefficient is derived as

$$\beta = -\frac{\log \frac{P_{\min}}{p_t}}{\log R_{max}}, \quad (1)$$

Moreover, measured results in [6] imply that the shadowing effect has few impact on the fractal coverage characteristics in cellular scenarios. As a consequence, the Rayleigh fading model is considered in this paper, but the shadowing effect is ignored in wireless channels [18], [19], [23].

D. Coverage Boundary Model

In this paper, the cell coverage area in a cellular system is configured as the expected percentage of area within a cell that has received power above a given minimum threshold [9]. Based on results in [6], the coverage boundary of cellular scenario has the fractal characteristic, *i.e.,* the distance distribution between the SBS and the coverage boundary presents the fractal characteristic in the angle domain. Hence, the fractal small cell defined as the coverage boundary presents the fractal characteristic in the angle domain, *i.e.,* Hurst effect. In [24], an alpha-stable distribution with the heavy-tail characteristic is applied to fit the distance from the cellular coverage boundary to the base station, which further confirms the heavy-tail effect and fractal characteristics of the cellular boundary in angle domain. However, most of alpha-stable distributions have not closed forms. It is difficult to derive and analyze the performance of fractal cellular regions, e.g., the coverage probability, based on the alpha-stable distributions. Pareto distributions have the heavy-tail and fractal characteristics in mathematics and can be expressed by a closed form. Hence, Pareto distributions are widely used to analyze the performance of wireless networks with heavy-tail and fractal characteristics [25]. To overcome the problem without closed forms in alpha-stable distributions, in this paper the Pareto distribution has been used to model the distances between the SBS and the coverage boundary of fractal small cell, whose probability density function (PDF) is expressed by [26]

$$f_{R_{\max}}(R_{\max}) = \begin{cases} \frac{\varepsilon}{\nu^{-\varepsilon}-\psi^{-\varepsilon}} {R_{\max}}^{-(\varepsilon+1)}, & v \le R_{\max} \le \psi \\ 0, & otherwise \end{cases}, \quad (2)$$

where $\varepsilon \in (1, 2]$ is the fractal parameter and reflects the heaviness of the distribution tail. When the value of fractal parameter ε is closer to 1, the distribution tail of $R_{\max}$ becomes heavier. To estimate the fractal parameter ε in practice, the Hurst parameter H, which is widely used for evaluating the fractal characteristic in practice [27], is used to derive the fractal parameter ε as follows [28]

$$\varepsilon = 3 - 2H. \quad (3)$$

Moreover, the Hurst parameter H can be estimated in practice by the Periodogram Method, the Rescaled Adjusted Range Statistic (R/S) Method and the Variance-Time Analysis Method [29]. For example, the value of Hurst parameter in urban area is estimated as 0.9 from the measured data in [6]. Based on (2), the fractal parameter ε can be configured as 1.2 for (1). This result implies slower decaying in the tail of PDF curve and more burstiness in the defined distances between the coverage boundary and the BS. Moreover, if the value of ε is smaller, then the fractal characteristic is stronger in Pareto distributions. ν represents the distance between the nearest coverage boundary location and the BS, *i.e.,* the minimum of $R_{\max}$, and ψ represents the farthest coverage boundary location and the BS, *i.e.,* the maximum of $R_{\max}$, respectively.

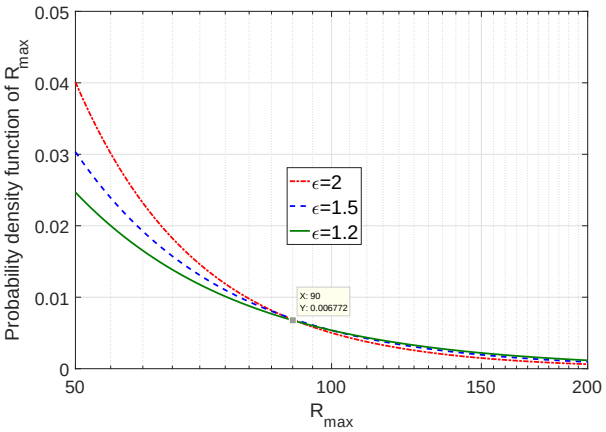

Fig. 2. PDF of the distance R_{max} considering different values of ε .

Fig. 2 shows the PDF of $R_{\max}$ with respect to the distance variable considering different fractal parameters ε. When the fractal parameter ε is fixed, the PDF of $R_{\max}$ decreases with increasing values of $R_{\max}$. When the distance variable $R_{\max}$ is less than 90 meters, the PDF of $R_{\max}$ increases with the increase of the fractal parameter ε. When distance variable $R_{\max}$ is larger than or equal to 90 meters, the PDF of $R_{\max}$ decreases with the increase of the fractal parameter.

This article has been accepted for publication in a future issue of this journal, but has not been fully edited. Content may change prior to final publication. Citation information: DOI 10.1109/TCOMM.2018.2849391, IEEE Transactions on Communications

III. Wireless Fractal Small Cell Network Models

Based on the fractal coverage characteristic of small cells, the coverage probability, the average achievable rate of a typical user and the area spectral efficiency are derived for small cell networks in the following section.

A. Coverage Probability

We assume that the channel power for the direct link from the serving BS SBS_0 to the typical user US_0 is denoted by $h_{0,0}$, the direct link is denoted by $g_{k,0}$. In this paper, we assume perfect CSI and focus on zero-forcing precoding, under which for Rayleigh fading it can be argued that the channel power distributions of both direct and the interfering links follow the Gamma distribution. It can therefore be shown that for zero forcing $h_{0,0} \sim Gamma(\Delta, 1)$, $g_{k,0} \sim Gamma(N_r, 1)$, where $\Delta = N_t - N_r + 1$ [30]. Then the receive signal model of a typical user US_0 is expressed by

$$y_0 = p_t h_{0,0} {r_0}^{-\beta} + \sum_{SBS_k \in \Phi_I / C_0} p_t g_{k,0} {r_k}^{-\beta} \ , \qquad (4)$$

where $\beta = -\frac{\log \frac{P_{\min}}{p_t}}{\log D}$, Φ_I / C_0 is the set of interfering SBSs corresponding to the fractal small cell. Considering the OFDM and frequency reuse techniques in small cell networks, there are only $1/\delta$th of SBSs using the same transmission frequency which interferes with the specified user.Based on the results of [31], the co-channel interfering signals can be assumed to be statistically independent in this paper. Hence, the density of interfering SBSs is denoted by $\lambda_I = \frac{\lambda_B}{\delta}$ and the set of interfering SBSs is denoted by $\Phi_I (\Phi_I \subset \Phi_B)$.

Since users are uniformly distributed in the coverage of fractal small cells, the distance between the typical user US_0 and SBS_0 is denoted by r_0, and the PDF of r_0 is:

$$f_{r_0}(r) = \begin{cases} \frac{2r}{R_{\max}^2}, & 0 < r \le R_{\max} \\ 0, & r > R_{\max} \end{cases} \ , \qquad (5)$$

where $r_0 = \eta R_{\max}$, and $\eta (0 < \eta \le 1)$, is the distribution coefficient. When $\eta = 1$, typical user is located at the coverage boundary of fractal small cells. Based on results in [32], the PDF of η is derived by

$$\begin{aligned} f_\eta(\eta) &= \frac{dP(\frac{r}{R_{\max}} < \eta)}{d\eta} \\ &= \frac{d\left(\int_0^{\eta R_{\max}} \frac{2r}{{R_{\max}}^2} dr \right)}{d\eta} = 2\eta \ , \quad 0 < \eta \le 1 \ . \end{aligned} \qquad (6)$$

Considering the interference-limited scenarios in this paper, the maximum-ratio transmission/maximum-ratio combining (MRT/MRC) scheme is adopted in small cell networks. The SIR of the user US_0 is expressed by

$$SIR_0 = \frac{p_t h_{0,0} {r_0}^{-\beta}}{\sum_{SBS_k \in \Phi_I / C_0} p_t g_{k,0} {r_k}^{-\beta}}, \qquad (7)$$

$$I_{agg} = \sum_{SBS_k \in \Phi_I / C_0} p_t g_{k,0} {r_k}^{-\beta}, \qquad (8)$$

where I_{agg} is the interference aggregated at the user US_0.

In this paper, the coverage probability for a typical user US_0 associated with SBS_0 is configured with the condition that the SIR of the user US_0 is larger than a given threshold T. Therefore, the probability of user US_0 coveraged by SBS_0 is expressed by

$$P_{\text{cov}}^{SBS}(T) = P(SIR_0 > T), \qquad (9)$$

Substitute (7) into (9), the probability $P(SIR_0 > T)$ is extended as

$$P_{\text{cov}}^{SBS}(T) = \frac{p_t h_{0,0} {r_0}^{-\beta}}{\sum_{SBS_k \in \Phi_I / C_0} p_t g_{k,0} {r_k}^{-\beta}} > T, \qquad (10)$$

The distribution of $h_{0,0}$ is

$$f_{h_{0,0}}(h) = \begin{cases} \frac{h^{\Delta-1} e^{-h}}{(\Delta-1)!}, & h > 0 \\ 0, & h \le 0 \end{cases} \ , \qquad (11)$$

where $\Delta = N_t - N_r + 1$.

Substitute (8) and (11) into (10), the probability $P(SIR_0 > T)$ is further derived by

$$\begin{aligned} P_{\text{cov}}^{SBS}(T) &= P(SIR_0 > T) \\ &= P(\frac{p_t h_{0,0} {r_0}^{-\beta}}{I_{agg}} > T) \\ &= P(h_{0,0} > p_t^{-1} T {r_0}^{\beta} I_{agg}) \\ &= \mathbb{E}_{r_0}[P(g_0 > p_t^{-1} T {r_0}^{\beta} I_{agg} | r_0)] \end{aligned} \ , \qquad (12)$$

with

$$\begin{aligned} & P(h_{0,0} > p_t^{-1} T {r_0}^{\beta} I_{agg} | r_0) \\ &= \mathbb{E}_{I_{agg}} \left\{ \sum_{n=0}^{\Delta-1} \frac{[T I_{agg} {r_0}^{\beta} p_t^{-1}]^n}{n!} e^{-T {r_0}^{\beta} p_t^{-1} I_{agg}} \right\} \\ &= \mathbb{E}_{I_{agg}} \left\{ \sum_{n=0}^{\Delta-1} \frac{[T {r_0}^{\beta} p_t^{-1}]^n}{n!} (I_{agg})^n e^{-T {r_0}^{\beta} p_t^{-1} I_{agg}} \right\} \\ &= \sum_{n=0}^{\Delta-1} \frac{[-T {r_0}^{\beta} p_t^{-1}]^n}{n!} \mathcal{L}_{I_{agg}}^{(n)} (T {r_0}^{\beta} p_t^{-1}) \end{aligned} \ , \qquad (13)$$

where $\mathcal{L}_{I_{agg}}^{(n)} (T {r_0}^{\beta} p_t^{-1})$ is the n order derivative of the Laplace transform over the aggregated interference I_{agg}.

Theorem 1: Based on the definition of the Laplace transform, the Laplace transform over the aggregated interference

I_{agg} is derived by

$$\mathcal{L}_{I_{agg}}(s)=\exp\left[-s^{\frac{2}{\beta}}(p_t)^{\frac{2}{\beta}}\lambda_I\frac{2\pi}{\beta}\sum_{m=1}^{N_r}\binom{N_r}{m}\cdot B_a^1(N_r-m+\tfrac{2}{\beta},m-\tfrac{2}{\beta})\right], \quad (14)$$

where $a=\frac{1}{1+s\frac{p_t}{N_t}r_0{}^{-\beta}}$, and $B_a^1(x,y)$ is the upper incomplete beta function, *i.e.,* $B_a^1(N_r-m+\frac{2}{\beta},m-\frac{2}{\beta})=\int_a^1 t^{N_r-m+\frac{2}{\beta}-1}(1-t)^{m-\frac{2}{\beta}-1}dt$.

Proof: Theorem 1 is proved by Appendix A.

Substitute (14) and $s=Tr_0^{\beta}p_t^{-1}$ into (13), based on the anisotropic path loss model, the coverage probability for the typical user US_0 in the service area of SBS_0 is further derived by

$$\begin{aligned}
&P_{\mathrm{cov},l_{\mathrm{A}}}^{SBS}(T)=P(SIR_0>T)\\
&=\mathbb{E}_{r_0}\left[\sum_{n=0}^{\Delta-1}\frac{[-Tr_0{}^{\beta}p_t^{-1}]^n}{n!}\mathcal{L}_{I_{agg}}^{(n)}(Tr_0{}^{\beta}p_t^{-1})\right]\\
&\overset{(a)}{=}\mathbb{E}_{R_{\max}}\mathbb{E}_{\eta}\left[\sum_{n=0}^{\Delta-1}\frac{[-T(\eta R_{max})^{\beta}p_t^{-1}]^n}{n!}\right.\\
&\left.\cdot\mathcal{L}_{I_{agg}}^{(n)}[T(\eta R_{max})^{\beta}p_t^{-1}]|\eta,R_{max}\right], \quad (15)\\
&=\sum_{n=0}^{\Delta-1}\int_{\nu}^{\psi}\frac{\varepsilon}{R_{\max}{}^{\varepsilon+1}(\nu^{-\varepsilon}-\psi^{-\varepsilon})}\\
&\cdot\int_0^1\frac{2\eta[-T(\eta R_{\max})^{\beta}p_t^{-1}]^n}{n!}\\
&\cdot\mathcal{L}_{I_{agg}}^{(n)}\left[T(\eta R_{\max})^{\beta}p_t^{-1}\right]d\eta dR_{\max}
\end{aligned}$$

where (a) is the substitution operation $r_0=\eta R_{\max}$, $\mathcal{L}_{I_{agg}}^{(n)}(s)$ is the n order derivative of the Laplace transform over the aggregated interference. Based on the lemma 3 in [33], $\mathcal{L}_{I_{agg}}^{(n)}(s)$ is expressed as

$$\begin{aligned}
&\mathcal{L}_{I_{agg}}^{(n)}(s)=\tfrac{d^n}{ds^n}\mathcal{L}_{I_{agg}}(s)\\
&=\exp\left[\Delta(s)\right]\cdot\sum_{\bar{m}\in M}C(\bar{m})\prod_{i=1}^{n}\left[\Delta^{(i)}(s)\right]^{m_i}, \quad (16)
\end{aligned}$$

with

$$C(\bar{m})=\frac{n!}{\Pi_k(m_k!(k!)^{m_k})},k=1,2,\cdots,n, \quad (17)$$

$$\Delta(s)=-s^{\frac{2}{\beta}}p_t{}^{\frac{2}{\beta}}\lambda_I\frac{2\pi}{\beta}\sum_{m=1}^{N_r}\binom{N_r}{m}B_a^1(N_r-m+\frac{2}{\beta},m-\frac{2}{\beta}), \quad (18)$$

$$\Delta^{(n)}(s)=\frac{2\pi\lambda_I}{\beta}(-1)^n\frac{(N_r+n-1)!}{(N_r-1)!}s^{\frac{2}{\beta}-n}B_a^1(N_r+\frac{2}{\beta},n-\frac{2}{\beta}), \quad (19)$$

$$a=\frac{1}{1+sp_tr_0^{-\beta}}, \quad (20)$$

where $\sum_{i=1}^{n}i\cdot m_i=n$, $i=1,2...n$, $\bar{m}=(m_1,m_2,\cdots m_n)$.

When the path loss model is configured as the isotropic path loss model, the coverage probability for the typical user in the service area of SBS_0 is simplified as

$$\begin{aligned}
P_{\mathrm{cov},l_{\mathrm{I}}}^{SBS}(T)=&\sum_{n=0}^{\Delta-1}\int_v^{\varphi}\int_0^1 2\eta\frac{\varepsilon[-T(\eta R_{\max})^{\alpha}p_t^{-1}]^n}{R_{\max}{}^{\varepsilon+1}(\nu^{-\varepsilon}-\psi^{-\varepsilon})n!}\\
&\cdot\mathcal{L}_{I_{agg}}^{(n)}[T(\eta R_{\max})^{\alpha}p_t^{-1}]d\eta dR_{\max}
\end{aligned}, \quad (21)$$

where α is the path loss coefficient used for the isotropic path loss model and is a constant as $\alpha=4$. The results for this isotropic path loss model are briefly presented here for the purpose of comparison in analytical simulations.

B. Average Achievable Rate

Based on the coverage probability of a typical user, the average achievable rate of a typical user can easily be expressed by

$$\Lambda=\mathbb{E}[\log(1+SIR_0)], \quad (22)$$

Substitute (7) into (22), the average achievable rate of a typical user is derived by

$$\Lambda=\mathbb{E}_{R_{max},\eta}\left[\mathbb{E}_{\mathbf{h},\mathbf{\Phi}_I}\left[\log(1+\frac{h_{0,0}r_0^{-\beta}}{\sum_{SBS_k\in\Phi_I/C_0}g_{k,0}r_k{}^{-\beta}})|R_{max},\eta\right]\right], \quad (23)$$

Based on the result of Lemma 1 in [34], we have the following result:

$$\begin{aligned}
&\mathbb{E}_{\mathbf{h},\mathbf{g},\Phi_I}\left[\log(1+\frac{h_{0,0}r_0^{-\beta}}{\sum_{SBS_k\in\Phi_I/C_0}g_{k,0}r_k{}^{-\beta}})|r_0\right]\\
&=\int_0^{\infty}\frac{1-\mathbb{E}_{h_{0,0}}\left[e^{-zh_{0,0}}\right]}{z}\mathbb{E}_{\mathbf{g_{k,0}},\Phi_I}\left[e^{-z\sum_{SBS_k\in\Phi_I/C_0}g_{k,0}r_k{}^{-\beta}r_0^{\beta}}\right]\\
&\overset{(a)}{=}\int_0^{\infty}\frac{1-(1+z)^{-\Delta}}{z}\mathbb{E}_{\Phi_I}\left[\prod_{SBS_k\in\Phi_I/C_0}\frac{1}{(1+zr_k{}^{-\beta}r_0^{\beta})^{N_r}}\right]dz,\\
&\overset{(b)}{=}\int_0^{\infty}\frac{1-(1+z)^{-\Delta}}{z}e^{-2\pi\lambda_I\int_{r_0}^{\infty}\left(1-\frac{1}{(1+zy^{-\beta}r_0^{\beta})^{N_r}}\right)ydy}dz\\
&\overset{(c)}{=}\int_0^{\infty}\frac{1-(1+z)^{-\Delta}}{z}e^{-\pi\lambda_Iz^{\frac{2}{\beta}}r_0^2\int_{z^{-\frac{2}{\beta}}}^{\infty}\left(1-\frac{1}{(1+w^{-\frac{\beta}{2}})^{N_r}}\right)dw}dz
\end{aligned} \quad (24)$$

where (a) is the operation based on the result of Lemma 1 in [34], (b) is the operation based on the probability generating functional (PGFL) of Poisson point processes, (c) is the variable substitution, *i.e.,* $w^{-\frac{\beta}{2}}=zy^{-\beta}r_0^{\beta}$.

Let $1-(1+w^{-\frac{\beta}{2}})^{-1}=t$, (24) is denoted by

$$\begin{aligned}
&\mathbb{E}_{\mathbf{h},\mathbf{g},\mathbf{\Phi}_I}\left[\log(1+\frac{h_{0,0}r_0^{-\beta}}{\sum_{SBS_k\in\Phi_I/C_0}g_{k,0}r_k{}^{-\beta}})|r_0\right]\\
&=\int_0^{\infty}\frac{1-(1+z)^{-\Delta}}{z}\exp\left[-\pi\lambda r_0^2z^{\frac{2}{\beta}}\right.\\
&\left.\cdot\int_0^{\frac{z}{1+z}}(1-(1-t)^{N_r})(1-t)^{\frac{2}{\beta}-1}t^{-\frac{2}{\beta}-1}dt\right]dz
\end{aligned}, \quad (25)$$

Let $\Theta = z^{\frac{2}{\beta}} \frac{2}{\beta} \int_0^{\frac{z}{1+z}} (1-(1-t)^{N_r})(1-t)^{\frac{2}{\beta}-1} t^{-\frac{2}{\beta}-1} dt$, we derive the following result:

$$\begin{aligned}
&\Theta = z^{\frac{2}{\beta}} \tfrac{2}{\beta} \textstyle\int_0^{\frac{z}{1+z}} (1-t)^{\frac{2}{\beta}-1} \cdot t^{-\frac{2}{\beta}-1} dt \\
&-z^{\frac{2}{\beta}} \tfrac{2}{\beta} \textstyle\int_0^{\frac{z}{1+z}} (1-t)^{N_r+\frac{2}{\beta}-1} \cdot t^{-\frac{2}{\beta}-1} dt \\
&= z^{\frac{2}{\beta}} t^{-\frac{2}{\beta}} \left[(1-t)^{N_r+\frac{2}{\beta}-1} - (1-t)^{\frac{2}{\beta}}\right]\Big|_0^{\frac{z}{1+z}} \\
&+z^{\frac{2}{\beta}} (N_r + \tfrac{2}{\beta} - 1) \textstyle\int_0^{\frac{z}{1+z}} t^{-\frac{2}{\beta}} (1-t)^{N_r+\frac{2}{\beta}-2} dt \\
&= -1 + (1+z)^{-N_r+1} + z^{\frac{2}{\beta}} (N_r + \tfrac{2}{\beta} - 1) \\
&\cdot B_0^b(1-\tfrac{2}{\beta}, N_r + \tfrac{2}{\beta} - 1) \\
&\overset{(d)}{=} -1 + (1+z)^{-N_r+1} + z^{\frac{2}{\beta}} N_r B_0^b(1-\tfrac{2}{\beta}, N_r + \tfrac{2}{\beta})
\end{aligned} \tag{26}$$

where (d) is the operation based on the beta function, *i.e.,* $B(x, y+1) = B(x,y) \cdot \frac{y}{x+y}$, $B_0^b(x,y)$ is the lower incomplete beta function, $b = \frac{z}{1+z}$, $B_0^b(1-\frac{2}{\beta}, N_r + \frac{2}{\beta}) = \int_0^b t^{-\frac{2}{\beta}} (1-t)^{N_r+\frac{2}{\beta}-1} dt$.

Substitute (26) into (25), we obtain the following result:

$$\begin{aligned}
&\mathbb{E}_{\mathbf{h},\mathbf{g},\mathbf{\Phi}_I}\left[\log(1 + \frac{h_{0,0} r_0^{-\beta}}{\sum_{SBS_k \in \Phi_I / C_0} g_{k,0} r_k^{-\beta}}) | r_0\right], \\
&= \textstyle\int_0^{\infty} \frac{1-(1+z)^{-\Delta}}{z} \exp[-\pi \lambda_I r_0^2 \Theta] dz
\end{aligned} \tag{27}$$

Substitute $r_0 = \eta R_{\max}$ into (23), the average achievable rate of a typical user is derived by

$$\begin{aligned}
&\Lambda \\
&= \mathbb{E}_{R_{\max}} \mathbb{E}_{\eta} \left[\textstyle\int_0^{\infty} \frac{1-(1+z)^{-\Delta}}{z} \exp[-\pi \lambda_I (\eta R_{\max})^2 \Theta] dz\right] \\
&= \left[\textstyle\int_v^{\varphi} \frac{\varepsilon}{R_{\max}^{\varepsilon+1} (\nu^{-\varepsilon} - \psi^{-\varepsilon})} \int_0^{\infty} \frac{1-(1+z)^{-\Delta}}{z}\right. \\
&\left. \cdot \textstyle\int_0^1 2\eta \exp[-\pi \lambda_I R_{\max}^2 \Theta \eta^2]\right] d\eta dz dR_{\max}, \\
&= \left\{\textstyle\int_0^{\infty} \frac{[1-(1+z)^{-\Delta}]\varepsilon}{z(\nu^{-\varepsilon} - \psi^{-\varepsilon})\lambda_I \Theta \pi} \cdot \left[\frac{v^{-\varepsilon-2} - \psi^{-\varepsilon-2}}{\varepsilon+2}\right.\right. \\
&\left.\left. + \frac{(\pi \lambda_I \Theta)^{\frac{\varepsilon+2}{2}} \left[\Gamma[-\frac{\varepsilon+2}{2}, \pi \lambda_I \Theta \psi^2] - \Gamma[-\frac{\varepsilon+2}{2}, \pi \lambda_I \Theta v^2]\right]}{2}\right]\right\} dz
\end{aligned} \tag{28}$$

with

$$\Theta = (1+z)^{-\Delta+1} + z^{\frac{2}{\beta}} N_r B_0^b(1-\frac{2}{\beta}, N_r + \frac{2}{\beta}) - 1, \tag{29}$$

$$\begin{aligned}
&B_0^b(1-\frac{2}{\beta}, N_r + \frac{2}{\beta}) = \int_0^{\frac{z}{1+z}} t^{-\frac{2}{\beta}} (1-t)^{N_r+\frac{2}{\beta}-1} dt \\
&b = \frac{z}{1+z}
\end{aligned}, \tag{30}$$

$$\Gamma(-y, x) = \int_x^{\infty} \left[\frac{e^{-t} - \sum_{i=0}^{n} (-1)^i \frac{t^i}{i!}}{t^{y+1}}\right] dt, \quad [n = \lfloor \mathrm{Re}\, y \rfloor], \tag{31}$$

where $B_0^b(x,y)$ is the lower incomplete beta function, $\mathrm{Re}\, y$ is the real part of the complex number y, and $\lfloor x \rfloor$ is the integral part of the real number x.

Theorem 2: Considering the interference-limited scenarios, the lower bound of the average achievable rate of a typical user is derived by

$$\begin{aligned}
&\underline{\Lambda} = \left\{\textstyle\int_0^{\infty} \frac{(1-e^{-z\frac{\Delta-1}{\Delta}})\varepsilon}{z(\nu^{-\varepsilon} - \psi^{-\varepsilon})\lambda_I \Xi \pi} \cdot \left[\frac{v^{-\varepsilon-2} - \psi^{-\varepsilon-2}}{\varepsilon+2}\right.\right. \\
&\left.\left. + \frac{(\pi \lambda_I \Xi)^{\frac{\varepsilon+2}{2}} [\Gamma(-\frac{\varepsilon+2}{2}, \pi \lambda_I \Xi \psi^2) - \Gamma(-\frac{\varepsilon+2}{2}, \pi \lambda_I \Xi v^2)]}{2}\right]\right\} dz
\end{aligned}, \tag{32}$$

with

$$\Xi = -1 + e^{-z} + z^{\frac{2}{\beta}} \gamma(1-\frac{2}{\beta}, z), \tag{33}$$

$$\Gamma(-y, x) = \int_x^{\infty} \left[\frac{e^{-t} - \sum_{i=0}^{n} (-1)^i \frac{t^i}{i!}}{t^{y+1}}\right] dt, \quad [n = \lfloor \mathrm{Re}\, y \rfloor], \tag{34}$$

where $\gamma(y,x) = \int_0^x t^{y-1} e^{-t} dt$ is the lower incomplete gamma function.

Proof: Theorem 2 is proved in Appendix B.

C. Area Spectral Efficiency

In conventional cellular network models, e.g., assuming with regular hexagon cellular coverage models and PVT random cellular coverage models, users are assumed to be seamlessly covered. However, in real propagation scenarios the coverage boundary of SBSs is irregular and some edge areas of adjacent SBSs are unavoidably omitted in cellular networks. Considering the fractal characteristic of coverage boundary, in this paper the small cell network is modeled as a type of non-seamless coverage cellular network in urban environments.

In this paper, the average received wireless signal power at the cell coverage boundary in a cellular system is equal to the minimum power threshold $P_{\min}$(dBm). Hence, we define the average probability that a typical user can not associate with small cell networks as

$$\begin{aligned}
&P_{no_Ass} \\
&= \mathbb{E}[P((p_t R_1^{-\beta} < P_{\min}) \cap \cdots (p_t R_n^{-\beta} < P_{\min}) \cap \cdots)],
\end{aligned} \tag{35}$$

where R_n is the distance from the typical user to the $n-th$ closest SBS in PPP small cell networks, $p_t R_n^{-\beta}$ is the average received wireless signal power of the typical user from the $n-th$ closest SBS, and $P_{\min}$ is the average received wireless signal power at the small cell coverage boundary.

Based on the definition of small cell coverage boundary,

This article has been accepted for publication in a future issue of this journal, but has not been fully edited. Content may change prior to final publication. Citation information: DOI 10.1109/TCOMM.2018.2849391, IEEE Transactions on Communications

we can convert equation (35) to

$$\begin{aligned}&\mathbb{E}[P((p_tR_1^{-\beta}<P_{\min})\cap\cdots(p_tR_n^{-\beta}<P_{\min})\cap\cdots)]\\&=\mathbb{E}_{\beta}\mathbb{E}_{R_{\max}}[P((p_tR_1^{-\beta}<p_tR_{\max}^{-\beta})\cap\\&\cdots(p_tR_n^{-\beta}<p_tR_{\max}^{-\beta})\cap\cdots)\,|\beta,R_{\max}]\\&=\mathbb{E}_{\beta}\mathbb{E}_{R_{\max}}[P((R_1>R_{\max})\cap\\&(R_2>R_{\max})\cap\cdots(R_n>R_{\max})\cap\cdots)\,|R_{\max}]\end{aligned}, \tag{36}$$

In PPP small cell networks, $R_1<R_2<\cdots<R_n<\cdots$, (36) can be further convert to

$$P_{no\_Ass}=\mathbb{E}_{R_{\max}}[P(R_1>R_{\max})\,|R_{\max}], \tag{37}$$

For a 2-D plane deployed by a homogeneous PPP small cell network with density λ_B, the probability that there is no SBS located inside an area with the radius $R_{\max}$ is denoted as $\exp(-\lambda_B\pi R_{\max}^2)$. Hence, $R_1>R_{\max}$ represents that there is no SBS located inside the circle area with the radius $R_{\max}$. Furthermore, the average probability that a typical user can not associate with small cell networks is derived by

$$P_{no\_Ass}=\mathbb{E}_{R_{\max}}[e^{-\lambda_B\pi R_{\max}^2}\,|R_{\max}], \tag{38}$$

Without loss of generality, the average probability that a typical user can associate with fractal small cell networks is expressed as

$$\begin{aligned}P_{Ass}&=1-P_{no\_Ass}\\&=1-\mathbb{E}_{\beta}\mathbb{E}_{R_{\max}}[e^{-\lambda_B\pi R_{\max}^2}\,|R_{\max}]\\&=1-\int_v^{\psi}e^{-\lambda_B\pi R_{\max}^2}\frac{\varepsilon}{\nu^{-\varepsilon}-\psi^{-\varepsilon}}R_{\max}^{-(\varepsilon+1)}dR_{\max}\\&=1-\frac{\varepsilon(\lambda_B\pi)^{\frac{\varepsilon}{2}}\left[\Gamma(-\frac{\varepsilon}{2},\lambda_B\pi v^2)-\Gamma(-\frac{\varepsilon}{2},\lambda_B\pi\psi^2)\right]}{2(\nu^{-\varepsilon}-\psi^{-\varepsilon})}\end{aligned}, \tag{39}$$

Hence, in area $\mathcal{A}$ the number of users which can associate with the fractal small cell networks is calculated as

$$N_{user}^{Ass}=P_{Ass}\lambda_u\mathcal{A}, \tag{40}$$

Moreover, the number of SBSs in area $\mathcal{A}$ is denoted as $N_{SBS}=\lambda_B\mathcal{A}$ and the average coverage area of a typical fractal small cell is expressed as

$$\begin{aligned}\mathcal{A}_{SBS}&=\mathbb{E}_{R_{\max}}\left[\int_0^{2\pi}\int_0^{R_{\max}}\frac{1}{2}r\cdot rd\theta dr\right]\\&=\mathbb{E}_{R_{\max}}[\pi R_{\max}^2]\\&=\frac{\varepsilon\left[\psi^{-\varepsilon+2}-\nu^{-\varepsilon+2}\right]\pi}{(2-\varepsilon)\left[\nu^{-\varepsilon}-\psi^{-\varepsilon}\right]}\end{aligned}, \tag{41}$$

The area spectral efficiency is one of metrics reflecting the network capacity, which is defined as the average throughput *per* Hz *per* unit area [35]–[37]. Therefore, the area spectral efficiency $(bits/s/Hz/m^2)$ of 5G fractal small cell networks is expressed as

$$\Omega=\frac{N_{user}^{Ass}\cdot\Lambda}{N_{SBS}\cdot\mathcal{A}_{SBS}}=\frac{P_{Ass}\lambda_u\Lambda}{\lambda_B\mathcal{A}_{SBS}}, \tag{42}$$

where Λ is the average achievable rate of a typical user in (28).

IV. Simulation Results and Discussions

To analyze the performance of small cell networks with fractal coverage characteristics, the coverage probability, the average achievable rate and the area spectral efficiency are simulated in this section. The analytical simulation is adopted as the default simulation method for this paper. Moreover, the Monto-Carlo (MC) simulation results are used to compare with the analytical results in Fig. 5, Fig. 6, Fig. 10 and Fig. 11. The simulation default parameters are listed in Table I.

A. Coverage Probability Performance

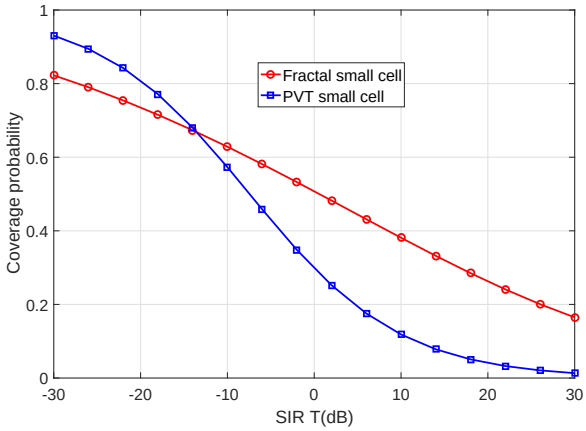

Fig. 3. Coverage probabilities with respect to the SIR threshold considering the fractal and PVT small cells.

Fig. 3 compares the coverage probabilities with respect to the SIR threshold considering the fractal and PVT small cells. When the SIR threshold is less than -18 dB, the coverage probability of PVT small cell is larger than the coverage probability of fractal small cell. When the SIR threshold is larger than or equal to -18 dB, the coverage probability of PVT small cell is less than or equal to the coverage probability of fractal small cell.

Fig. 4 illustrates the coverage probability of fractal small cell networks with respect to the SIR threshold considering different number of SBS antennas and users in a given resource block. For the sake of simplicity, the number of antennas at SBSs is configured to be same as the number of users in a given resource block. When the number of antennas is fixed, the coverage probability decreases with

This article has been accepted for publication in a future issue of this journal, but has not been fully edited. Content may change prior to final publication. Citation information: DOI 10.1109/TCOMM.2018.2849391, IEEE Transactions on Communications

TABLE I
SIMULATION DEFAULT PARAMETERS OF 5G SMALL CELL NETWORKS

Parameters	Description	Default value
λ_B	Density of SBSs	$\lambda_B = \frac{1}{\pi 100^2}(1/m^2)$
λ_u	Users density	$5\lambda_B$
δ	Frequency reuse factor	2
λ_I	Density of interfering SBSs	$\lambda_I = \frac{\lambda_B}{\delta}$
N_t	Number of SBSs transmission antennas	2
N_r	Number of users served by each BS in a given resource block	2
p_t	Transmission power of small cell	30dBm(1W)
P_{min}	Received power at coverage boundary	-110dBm
ε	Shape parameter of fractal coverage boundary	1.2

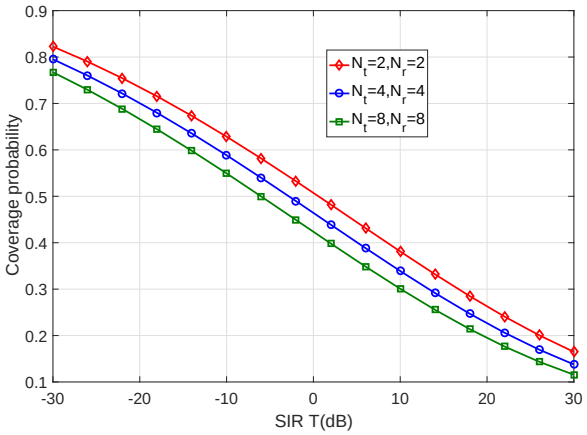

Fig. 4. Coverage probability of 5G fractal small cell networks with respect to the SIR threshold considering different number of SBS transmission antennas.

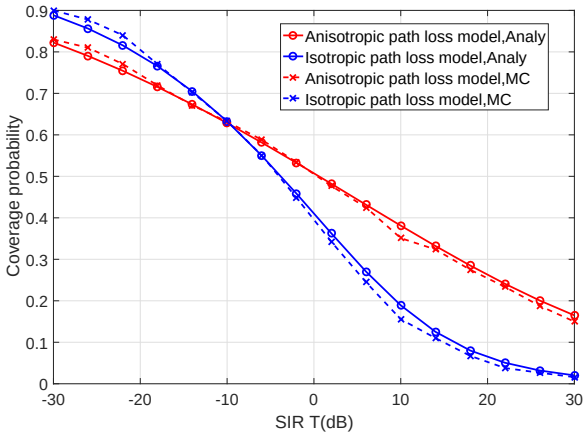

Fig. 6. Coverage probability of 5G fractal small cell networks with respect to the SIR threshold.

the increase of the SIR threshold. When the SIR threshold is fixed, the coverage probability decreases with the increase in the number of antennas.

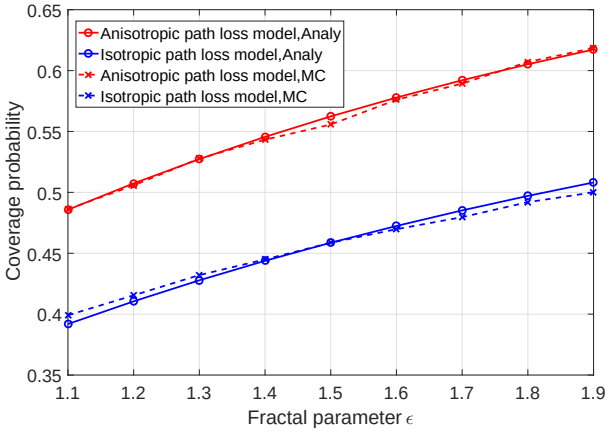

Fig. 5. Coverage probability with anisotropic and isotropic path loss models with respect to the fractal parameter.

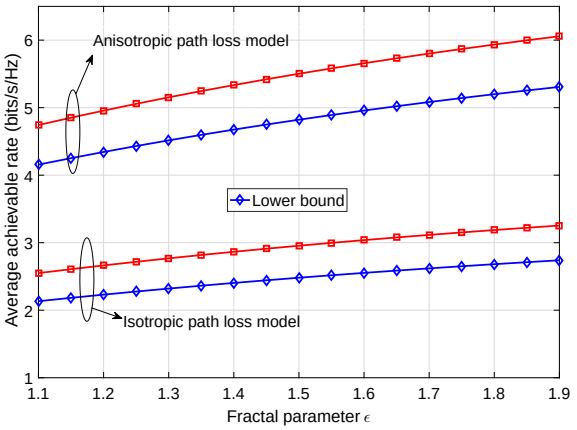

Fig. 7. Average achievable rate with respect to the fractal parameter ε considering different path loss models.

To validate the proposed coverage probability, the MC simulation is performed to compare with the analytical results in Fig. 5, in which "Analy" labels the analytical results and "MC" represents the MC simulation results.

This article has been accepted for publication in a future issue of this journal, but has not been fully edited. Content may change prior to final publication. Citation information: DOI 10.1109/TCOMM.2018.2849391, IEEE Transactions on Communications

Fig. 5 depicts the coverage probability with anisotropic and isotropic path loss models with respect to the fractal parameter ε. When the SIR threshold of fractal small cell networks is fixed at 0 dBm, the coverage probability with anisotropic and isotropic path loss models increases with the increase of the fractal parameter. When the fractal parameter ε is fixed, the coverage probability with anisotropic path loss model is larger than the coverage probability with isotropic path loss model.

Fig. 6 illustrates the coverage probability with respect to the SIR threshold considering anisotropic and isotropic path loss models in fractal small cell networks. When the SIR threshold is less than -10 dB, the coverage probability with isotropic path loss models is larger than the coverage probability with anisotropic path loss models. When the SIR threshold is larger than or equal to -10 dB, the coverage probability with isotropic path loss models is less than or equal to the coverage probability with anisotropic path loss models.

B. Average Achievable Rate Performance

Fig. 7 evaluates the average achievable rate with respect to the fractal parameter ε considering different path loss models. When the path loss model is fixed, The average achievable rate increases with the increase of fractal parameter ε. When the fractal parameter is fixed, the average achievable rate with the anisotropic path loss model is larger than the average achievable rate with the isotropic path loss model.

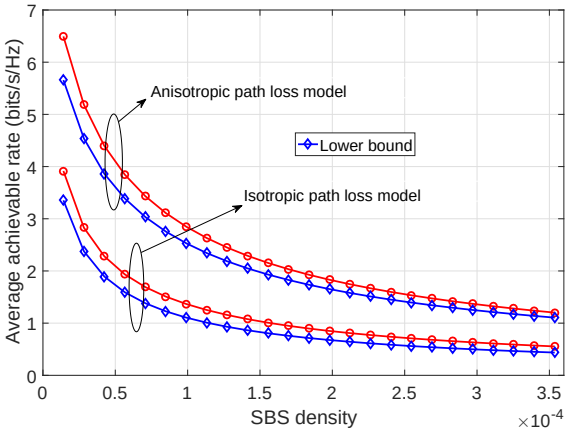

Fig. 8. Average achievable rate with respect to SBS density λ_B considering anisotropic and isotropic path loss models.

Fig. 8 evaluates the average achievable rate with respect to SBS density λ_B considering different path loss models. When the path loss model is fixed, the average achievable rate decreases with the increase of SBS density λ_B. When the SBS density is fixed, the average achievable rate with anisotropic path loss model is larger than the average achievable with isotropic path loss model. Moreover, the lower bound of the average achievable rate with the anisotropic path loss model is larger than the lower bound of the average achievable rate with the isotropic path loss model.

C. Area Spectral Efficiency Performance

Fig. 9 depicts the average association probability with respect to the SBS density λ_B considering different fractal parameters. When the fractal parameter is fixed, the average association probability increases with the increase of SBS density λ_B. When the SBS density λ_B is fixed, the average association probability increases with the decrease of the fractal parameter.

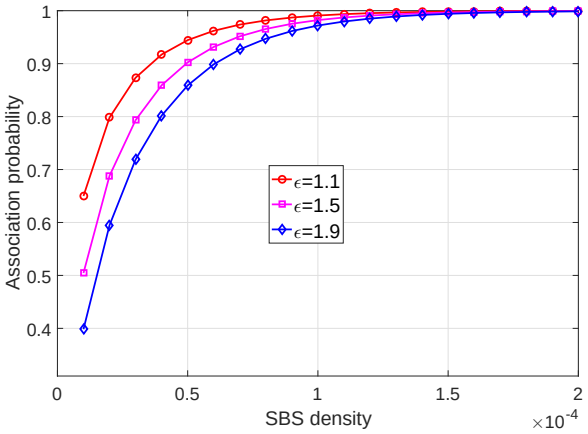

Fig. 9. Average association probability with respect to SBS density λ_B considering different fractal parameters.

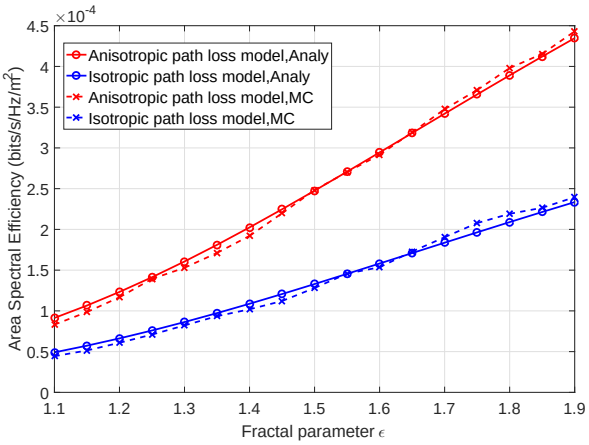

Fig. 10. Area spectral efficiency with respect to the fractal parameter considering anisotropic and isotropic path loss models.

This article has been accepted for publication in a future issue of this journal, but has not been fully edited. Content may change prior to final publication. Citation information: DOI 10.1109/TCOMM.2018.2849391, IEEE Transactions on Communications

Fig. 10 compares the area spectral efficiency with respect to the fractal parameter considering anisotropic and isotropic path loss models. When the path loss model is fixed, the area spectral efficiency increases with the increase of the fractal parameters in fractal small cell networks. When the fractal parameter is fixed, the area spectral efficiency with anisotropic path loss model is larger than the area spectral efficiency with isotropic path loss model.

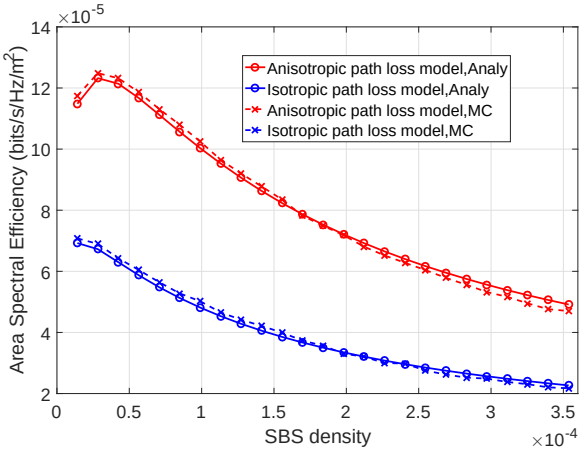

Fig. 11. Area spectral efficiency with respect to SBS density λ_B considering anisotropic and isotropic path loss models.

Fig. 11 shows the area spectral efficiency with respect to the SBS density λ_B considering anisotropic and isotropic path loss models. When the anisotropic path loss model is adopted, the area spectral efficiency firstly increases with the increase of SBS density λ_B and then decreases with the increase of the SBS density λ_B when the SBS density is larger than a given threshold. When the isotropic path loss model is adopted, the area spectral efficiency decreases with the increase of the SBS density λ_B. When the SBS density λ_B is fixed, the area spectral efficiency with anisotropic path loss model is larger than the area spectral efficiency with isotropic path loss model in fractal small cell networks.

V. Conclusions

Considering the anisotropic path loss in wireless channels of realistic cellular scenarios, small cell networks with wireless fractal coverage characteristics are investigated in this paper. Moreover, the coverage probability, the average achievable rate and the area spectral efficiency are derived to analyze the performance of fractal small cell networks. Furthermore, the lower bound of average achievable rate is derived by an analytical form. Analytical and MC simulation results indicate that the coverage probability with anisotropic path loss models has been overestimated in low SIR regimes and has been underestimated in high SIR regimes compared with the coverage probability with isotropic path loss models in fractal small cell networks. Moreover, the average achievable rate and area spectral efficiency with anisotropic path loss models have been underestimated compared with the average achievable rate and area spectral efficiency with isotropic path loss models in fractal small cell networks. Considering the impact of the anisotropic path loss on realistic cellular scenarios, most of performances, *e.g.,* the coverage probability, the average achievable rate and area spectral efficiency have to be re-evaluated for wireless cellular networks. Our results provide a tractable method to analyze the impact of anisotropic path loss on the performance of small cell networks with wireless fractal coverage characteristics.

Appendix A

Based on the definition of the Laplace transform, the derivation process of the aggregated interference is extended as follows:

$$\begin{aligned}
&\mathcal{L}_{I_{agg}}(s) = \left[e^{-sI_{agg}}\right] \\
&= \mathbb{E}_{\mathbf{\Phi_B},\mathbf{g}}\left\{\prod_{SBS_k\in\Phi_I/C_0}\exp(-sp_t r_k{}^{-\beta}g_{k,0})\right\} \\
&\overset{(a)}{=} \exp\left[-\int_r g\left[1-\exp(-sp_t r_k{}^{-\beta}g_k)\right]2\pi\lambda_I r dr\right], \\
&= \exp\left[-\int_r\left(\int_0^\infty \frac{g^{N_r-1}}{\Gamma(N_r)}e^{-g}(1-e^{-sp_t r^{-\beta}g})dg\right)\right. \\
&\quad \left.\cdot\, 2\pi\lambda_I r dr\right] \\
&= \exp\left[-\int_{r>r_0}\left(1-\frac{1}{(1+sp_t r^{-\beta})^{N_r}}\right)\lambda_I d(\pi r^2)\right]
\end{aligned} \tag{43}$$

where (a) follows PGFL in Poisson point processes.

Based on the Binomial theory, (43) is further derived by

$$\begin{aligned}
&L_{I_{agg}}(s) \\
&= \exp\left[-\int_{r>r_0}\frac{\sum_{m=1}^{N_r}\binom{N_r}{m}\left(sp_t r^{-\beta}\right)^m}{(1+sp_t r^{-\beta})^{N_r}}\right], \\
&= \exp\left[-\sum_{m=1}^{N_r}\binom{N_r}{m}\int_{r>r_0}\left(sp_t r^{-\beta}\right)^m\right. \\
&\left.\cdot\left(1+sp_t r^{-\beta}\right)^{N_r}\lambda_I d\left(\pi r^2\right)\right]
\end{aligned} \tag{44}$$

When $(1+sp_t r^{-\beta})^{-1}$ is substituted by t and $a = \frac{1}{1+sp_t r_0{}^{-\beta}}$, the Laplace transform of the aggregated interference is further derived by

$$\begin{aligned}
&L_{I_{agg}}(s) = \exp\left[-s^{\frac{2}{\beta}}(p_t)^{\frac{2}{\beta}}\lambda_I\frac{2\pi}{\beta}\sum_{m=1}^{N_r}\binom{N_r}{m}\right. \\
&\left.\cdot\int_{\frac{1}{1+sp_t r_0{}^{-\beta}}}^1 t^{N_r-m+\frac{2}{\beta}-1}(1-t)^{m-\frac{2}{\beta}-1}dt\right], \\
&= \exp\left[-s^{\frac{2}{\beta}}(p_t)^{\frac{2}{\beta}}\lambda_I\frac{2\pi}{\beta}\sum_{m=1}^{N_r}\binom{N_r}{m}\right. \\
&\left.\cdot B_a^1(N_r-m+\tfrac{2}{\beta},m-\tfrac{2}{\beta})\right]
\end{aligned} \tag{45}$$

Hence, the Theorem 1 is proved.

APPENDIX B

The average achievable rate of a typical user is extended by

$$\begin{aligned}\Lambda &= \mathbb{E}_{R_{\max},\eta}\left[\mathbb{E}_{\Phi_I/C_0,\mathbf{h},\mathbf{g}}\ [\log(1+SIR_0)|R_{\max},\eta]\right] \\ &= \mathbb{E}_{\beta,R_{\max},\eta}\left[\mathbb{E}_{\Phi_I/C_0,\mathbf{h},\mathbf{g}}\right. \\ &\left.\left[\log(1+\frac{1}{\sum\limits_{SBS_k\in\Phi_I/C_0}\frac{g_{k,0}}{h_{0,0}}r_k^{-\beta}r_0^{\beta}})|R_{\max},\eta\right]\right]\end{aligned}, \tag{46}$$

Based on the Jensen's inequality, $\mathbb{E}_{\Phi_I/C_0,\mathbf{h},\mathbf{g}}\left[\log(1+\frac{1}{\sum\limits_{SBS_k\in\Phi_I/C_0}\frac{g_{k,0}}{h_{0,0}}r_k^{-\beta}r_0^{\beta}})|R_{\max},\eta\right]$ is derived by

$$\begin{aligned}&\mathbb{E}_{\Phi_I/C_0,\mathbf{h},\mathbf{g}}\left[\log\left(1+\frac{1}{\sum\limits_{SBS_k\in\Phi_I/C_0}\frac{g_{k,0}}{h_{0,0}}r_k^{-\beta}r_0^{\beta}}\right)|r_0\right] \\ &\geq \mathbb{E}_{\Phi_I/C_0}\left[\log\left(\frac{1+\mathbb{E}_{\mathbf{h},\mathbf{g}}\left[\sum\limits_{SBS_k\in\Phi_I/C_0}\frac{g_{k,0}}{h_{0,0}}r_k^{-\beta}r_0^{\beta}\right]}{\mathbb{E}_{\mathbf{h},\mathbf{g}}\left[\sum\limits_{SBS_k\in\Phi_I/C_0}\frac{g_{k,0}}{h_{0,0}}r_k^{-\beta}r_0^{\beta}\right]}\right)|r_0\right],\end{aligned} \tag{47}$$

Considering that g_0 and g_k are independent of each other and have the identically distribution, we can derive $\mathbb{E}_{\mathbf{h},\mathbf{g}}\left[\sum\limits_{SBS_k\in\Phi_I/C_0}\frac{g_{k,0}}{h_{0,0}}r_k^{-\beta}r_0^{\beta}\right] = \mathbb{E}\left[\frac{1}{h_{0,0}}\right]\sum\limits_{SBS_k\in\Phi_I/C_0}\mathbb{E}[g_{k,0}]r_k^{-\beta}r_0^{\beta}$. Based on the properties of Gamma distribution, *i.e.,* $h_{0,0}\sim Gamma(\Delta,1)$ and $g_{k,0}\sim Gamma(N_r,1)$, we have $\mathbb{E}[g_k]=N_r$ and $\frac{1}{g_0}$ is governed by an inverse Gamma distribution, *i.e.,* $\frac{1}{g_0}\sim IGamma(\Delta,1)$. Due to the property of inverse Gamma distribution, $\mathbb{E}\left[\frac{1}{g_0}\right]=\frac{1}{\Delta-1}$ is derived. We can further derive $\mathbb{E}_{\mathbf{g}}\left[\sum\limits_{SBS_k\in\Phi_I/C_0}\frac{g_{k,0}}{h_{0,0}}r_k^{-\beta}r_0^{\beta}\right] = \mathbb{E}\left[\frac{1}{h_{0,0}}\right]\sum\limits_{SBS_k\in\Phi_I/C_0}\mathbb{E}[g_{k,0}]r_k^{-\beta}r_0^{\beta} = \frac{\Delta}{\Delta-1}\sum\limits_{SBS_k\in\Phi_I/C_0}r_k^{-\beta}r_0^{\beta}$. As a consequent, (47) is derived by

$$\begin{aligned}&\mathbb{E}_{\Phi_I/C_0,\mathbf{h},\mathbf{g}}\left[\log\left(1+\frac{1}{\sum\limits_{SBS_k\in\Phi_I/C_0}\frac{g_{k,0}}{h_{0,0}}r_k^{-\beta}r_0^{\beta}}\right)|\beta,r_0\right], \\ &\geq \mathbb{E}_{\Phi_I/C_0}\left[\log\left(1+\frac{\frac{\Delta-1}{\Delta}}{\sum\limits_{SBS_k\in\Phi_I/C_0}r_k^{-\beta}r_0^{\beta}}\right)\right]\end{aligned} \tag{48}$$

Based on the result in [34], (48) is further derived by

$$\begin{aligned}&\mathbb{E}_{\Phi_I/C_0}\left[\log\left(1+\frac{\frac{\Delta-1}{\Delta}}{\sum\limits_{SBS_k\in\Phi_I/C_0}r_k^{-\beta}r_0^{\beta}}\right)\right] \\ &\overset{(a)}{=}\int_0^{\infty}\frac{1-e^{-z\frac{\Delta-1}{\Delta}}}{z}\mathbb{E}\left[e^{-z\sum\limits_{SBS_k\in\Phi_I/C_0}r_k^{-\beta}r_0^{\beta}}\right]dz, \\ &\overset{(b)}{=}\int_0^{\infty}\frac{1-e^{-z\frac{\Delta-1}{\Delta}}}{z}\cdot e^{-2\lambda_I\pi\int_{r_0}\left(1-e^{-zy^{-\beta}r_0^{\beta}}\right)ydy}dz \\ &\overset{(c)}{=}\int_0^{\infty}\frac{1-e^{-z\frac{\Delta-1}{\Delta}}}{z}\cdot e^{-\lambda_I\pi r_0^2 z^{\frac{2}{\beta}}\int_{z^{-2/\beta}}(1-e^{-u^{-\frac{\beta}{2}}})du}dz\end{aligned} \tag{49}$$

where (a) is the operation based on the lemma 1 in [34], (b) is the PGFL in Poisson point processes and (c) is the substitution operation with $u^{-\frac{\beta}{2}}=zy^{-\beta}r_0^{\beta}$. Substitute (49) and (48) into (46), the lower bound of average achievable rate of a fractal small cell is derived by

$$\begin{aligned}\underline{\Lambda} &= \mathbb{E}_{R_{\max},\eta}\left[\int_0^{\infty}\frac{1-e^{-z\frac{\Delta-1}{\Delta}}}{z}\right. \\ &\left.\cdot e^{-\lambda_I\pi(\eta R_{\max})^2 z^{\frac{2}{\beta}}\int_{z^{-2/\beta}}(1-e^{-u^{-\frac{\beta}{2}}})du}dz\right] \\ &\overset{(d)}{=}\mathbb{E}_{R_{\max},\eta}\left[\int_0^{\infty}\frac{1-e^{-z\frac{\Delta-1}{\Delta}}}{z}\right. \\ &\left.\cdot e^{-\lambda_I\pi(\eta R_{\max})^2(-1+e^{-z}+z^{\frac{2}{\beta}}\gamma(1-\frac{2}{\beta},z))}dz\right] \\ &= \int_0^{\infty}\frac{(1-e^{-z\frac{\Delta-1}{\Delta}})\varepsilon}{z(\nu^{-\varepsilon}-\psi^{-\varepsilon})\lambda_I(-1+e^{-z}+z^{\frac{2}{\beta}}\gamma(1-\frac{2}{\beta},z))} \\ &\cdot\int_{\nu}^{\psi}\frac{1-e^{-\lambda_I\pi R_{\max}^2(-1+e^{-z}+z^{\frac{2}{\beta}}\gamma(1-\frac{2}{\beta},z))}}{R_{\max}^{\varepsilon+3}}dR_{\max}dz \\ &= \left\{\int_0^{\infty}\frac{(1-e^{-z\frac{\Delta-1}{\Delta}})\varepsilon}{z(\nu^{-\varepsilon}-\psi^{-\varepsilon})\lambda_I\Xi\pi}\cdot\left[\frac{v^{-\varepsilon-2}-\psi^{-\varepsilon-2}}{\varepsilon+2}\right.\right. \\ &\left.\left.+\frac{(\pi\lambda_I\Xi)^{\frac{\varepsilon+2}{2}}[\Gamma(-\frac{\varepsilon+2}{2},\pi\lambda_I\Xi\psi^2)-\Gamma(-\frac{\varepsilon+2}{2},\pi\lambda_I\Xi v^2)]}{2}\right]\right\}dz\end{aligned}, \tag{50}$$

with (51) and (52)

$$\Xi=-1+e^{-z}+z^{\frac{2}{\beta}}\gamma(1-\frac{2}{\beta},z), \tag{51}$$

$$\Gamma(-y,x)=\int_x^{\infty}\left[\frac{e^{-t}-\sum\limits_{i=0}^{n}(-1)^i\frac{t^i}{i!}}{t^{y+1}}\right]dt,\qquad [n=\lfloor\mathrm{Re}\,y\rfloor]\ , \tag{52}$$

where $\gamma(y,x)=\int_0^x t^{y-1}e^{-t}dt$ is the lower incomplete Gamma function, (d) is the substitution operation with $\gamma(y+1,x)=y\gamma(y,x)-x^ye^{-x}$ based on the property of lower incomplete function. Hence, the Theorem 2 is proved.

REFERENCES

[1] C. Stephen, *et al.* "*Ericson Mobility Report,*" Tech. Rep., Jun. 2015.

[2] Cisco, Visual Networking Index, "Global Mobile Data Traffic Forecast Update, 2009–2014," white paper, 2010.
[3] X. Ge, L. Pan, Q. Li, G. Mao and S. Tu, "Multi-Path Cooperative Communications Networks for Augmented and Virtual Reality Transmission," *IEEE Trans. Multim.*, vol 19, no. 10, pp. 2345–2358, Oct. 2017.
[4] X. Ge, S. Tu, G. Mao, *et al*. "5G Ultra-Dense Cellular Networks," *IEEE Wireless Commun.*, vol. 23, no. 1, pp. 72–79, Jun. 2016.
[5] C. Wang, F. Haider, X. Gao, *et al*. "Architecture and Key Technologies for 5G Wireless Communication Networks," *IEEE Commun. Mag.*, vol. 52, no. 2, pp. 122–130, Jun. 2016.
[6] X. Ge, Y. Qiu, J. Chen, *et al*. "Wireless Fractal Cellular Networks," *IEEE Wireless Commun.*, vol. 23, no. 5, pp.110–119, Oct. 2016.
[7] Z. Mulk, S. Hassan, "On Achievable Rates in Massive MIMO-based Hexagonal Cellular System with Pilot Contamination," in *Proc. IEEE VTC*, vol. 1, pp. 1–5, 2015.
[8] S. Kumar, S. Kalyani, L. Hanzo, *et al*. "Coverage Probability and Achievable Rate Analysis of FFR-Aided Multi-User OFDM-Based MIMO and SIMO Systems," *IEEE Trans. Commun.*, vol. 63, no. 10, pp. 3369–3381, Oct. 2015.
[9] J. G. Andrea, *Wireless communication,* Cambridge University Press, 2005.
[10] M. Haenggi, J. Andrews, F. Baccelli, *et al*. "Stochastic Geometry and Random Graphs for the Analysis and Design of Wireless Networks," *IEEE J. Sel. Areas Commun.*, vol. 27, no. 7, pp. 1029–1046, Sep. 2009.
[11] H. Zhang, S. Chen, L. Feng, "A Universal Approach to Coverage Probability and Throughput Analysis for Cellular Networks," *IEEE Trans. Veh. Technol.*, vol. 64, no. 9, pp. 4245–4256, Sep. 2015.
[12] X. Ge, B. Yang, J. Ye, *et al*. "Spatial Spectrum and Energy Efficiency of Random Cellular Networks," *IEEE Trans. Commun.*, vol. 63, no. 3, pp. 1019–1030, 2015.
[13] C. Li, J. Zhang, K. Letaief, "Throughput and Energy Efficiency Analysis of Small Cell Networks with Multi-Antenna Base Stations," *IEEE Trans. Wireless Commun.*, vol. 13, no. 5, pp. 2505–2517, May. 2014.
[14] H. Wang, X. Zhou, M. Reed, "Coverage and Throughput Analysis with a Non-Uniform Small Cell Deployment," *IEEE Trans. Wireless Commun.*, vol. 13, no. 4, pp. 2047–2059, Apr. 2014.
[15] H. Inaltekin, M. Chiang, H. Poor, *et al*. "On Unbounded Path-loss Models: Effect of Singularity on Wireless Network Performance," *IEEE J. Sel. Areas Commun.*, vol. 27, no. 7, pp. 1078–1092, Sep. 2009.
[16] D. Ming, P. wang, D. Perez, *et al*. "Performance Impact of LoS and NLoS Transmissions in Dense Cellular Networks," *IEEE Trans. Wireless Commun.*, vol. 15, no. 3, pp. 2365-2380, Mar. 2016.
[17] C. Galiotto, N. Pratas, N. Marchetti, *et al*. "A Stochastic Geometry Framework for LOS/NLOS Propagation in Dense Small Cell Networks," in *Proc. IEEE ICC*, pp. 2851–2856, 2015.
[18] X. Zhang, J. Andrews, "Downlink Cellular Network Analysis with Multi-Slope Path Loss Models," *IEEE Trans. Commun.*, vol. 63, no. 5, pp. 1881–1894, May. 2015.
[19] T. Han, Y. Han, X. Ge, *et al*. "Small Cell Offloading Through Cooperative Communication in Software-Defined Heterogeneous Networks," *IEEE Sensors Journal*, vol. 16, no. 20, pp. 7381–7392, Oct. 2016.
[20] Mandelbrot, Benot B, *The Fractal Geometry of Nature. Macmillan*, W. H. Freeman and Company, 1983.
[21] H. E. Hurst, R. P. Black, and Y. M. Simaika, *Long-Term Storage: An Experimental Study*, Constable, London, 1965.
[22] Keith Q.T. Zhang, *Wireless Communications: Principles, Theory and Methodology, First Edition*, John Wiley & Sons, Ltd. Published, 2016.
[23] C. Fan, Y. J. Zhang, and X. Yuan, "Dynamic Nested Clustering for Parallel PHY-layer Processing in Cloud-RANs," *IEEE Trans. Wireless Commun.*, vol. 15, no. 3, pp.1881–1894, Mar. 2016.
[24] X. Ge, M. Huang, J. Chen, *et al*. "Wireless Single Cellular Coverage Boundary Models," *IEEE Access*, vol. 4, pp. 3569–3577, Jul. 2016.
[25] Y. Tian, D. Han, L. Liu and Y. Fu, "A Self-similar Traffic Generation Model based on Time," in *Proc. IEEE International Symposium on MAPE*, pp. 160-163, Oct. 2017.
[26] P. Zhang, X. Gong, L. Guo, *et al*. "A New Fractal Point Process for Modeling Self-Similar Traffic," in *Proc. IEEE ICCT*, Oct. 1998.
[27] W. E. Leland, M. S. Taqqu, W. Willinger and D. V. Wilson, "On the Self-similar Nature of Ethernet Traffic (Extended Version)," *IEEE/ACM Trans. Netw*, vol. 2, no. 1, pp. 1-15, Feb. 1994.
[28] A. Popescu, "Traffic Self-similarity," in *Proc. IEEE ICT*, pp. 20–24, Jun. 2001.
[29] X. Ge, G. Zhu, and Y. Zhu, "On the Testing for Alpha-Stable Distributions of Network Traffc," *Comp. Commun.*, vol. 27, no. 5, pp. 447–57, Mar. 2004.
[30] H. Huang, C. B. Papadias, and S . Venkatesan, *MIMO Communication for Cellular Networks*, Springer, 2012.
[31] X. Yang, A. O. Fapojuwo, "Performance Analysis of Poisson Cellular Networks with Lognormal Shadowed Rayleigh fading," in *Proc. IEEE ICC*, pp. 1042-1047, May. 2014.
[32] D. Wang, J. Wang, X. You, *et al*. "Spectral Efficiency of Distributed MIMO Systems," *IEEE J. Sel. Areas Commun.*, vol. 31, no. 10, pp. 2112–2127, Oct. 2013.
[33] A. Gupta, H. Dhillon, S. Vishwanath, *et al*. "Downlink Coverage Probability in MIMO HetNets with Flexible Cell Selection," in *Proc. IEEE Globecom*, pp. 1534–1539, 2014.
[34] K. A. Hamdi, "A Useful Lemma for Capacity Analysis of Fading Interference Channels," *IEEE Trans. Commun.*, vol. 58, no. 2, pp. 411–416, Feb. 2010.
[35] Z. Chen, L. Qiu, X. Liang, "Area Spectral Efficiency Analysis and Energy Consumption Minimization in Multiantenna Poisson Distributed Networks," *IEEE Trans. Wireless Commun.*, vol. 15, no. 7, pp. 4862–4874, Jul. 2016.
[36] Y. Xin, D. Wang, J. Li, *et al*. "Area Spectral Efficiency and Area Energy Efficiency of Massive MIMO Cellular Systems," *IEEE Trans. Veh. Technol.*, vol. 65, no. 5, pp. 3243–3254, May. 2016.
[37] S. Zaidi, D. C. McLernon, M. Ghogho, "Breaking the Area Spectral Efficiency Wall in Cognitive Underlay Networks," *IEEE J. Sel. Areas Commun.*, vol. 32, no. 11, pp. 2205–2221, Nov. 2014.

Xiaohu Ge (M'09-SM'11) is currently a full Professor with the School of Electronic Information and Communications at Huazhong University of Science and Technology (HUST), China. He is an adjunct professor with with the Faculty of Engineering and Information Technology at University of Technology Sydney (UTS), Australia. He received his PhD degree in Communication and Information Engineering from HUST in 2003. He has worked at HUST since Nov. 2005. Prior to that, he worked as a researcher at Ajou University (Korea) and Politecnico Di Torino (Italy) from Jan. 2004 to Oct. 2005.

His research interests are in the area of mobile communications, traffic modeling in wireless networks, green communications, and interference modeling in wireless communications. He has published more than 200 papers in refereed journals and conference proceedings and has been granted about 25 patents in China. He received the Best Paper Awards from IEEE Globecom 2010. Dr. Ge served as the general Chair for the 2015 IEEE International Conference on Green Computing and Communications (IEEE GreenCom 2015). He serves as an associate editor for IEEE Wireless Communications, IEEE Transactions on Vehicular Technology and IEEE ACCESS, etc.

Xiaotong Tian received the B.E. degree in Communication Engineering from Hunan University (HNU), Changsha, China, in 2016. Now She is working toward the Masters degree in Huazhong University of Science and Technology (HUST), Wuhan, China.

Her research interests mainly include characteristic and performance analysis of wireless fractal cellular networks, energy efficiency of wireless cellular networks.

Yehong Qiu received her B.E. degree and M.S. degree in communication engineering from HUST in 2014 and 2017 respectively, is now serving as an intellectual property engineer in the Legal Affairs Department of Huawei Technology Co., Ltd.

Guoqiang Mao (S'98-M'02-SM'08-F'18) joined the University of Technology Sydney in February 2014 as Professor of Wireless Networking and Director of Center for Real-time Information Networks. Before that, he was with the School of Electrical and Information Engineering, the University of Sydney. He has published about 200 papers in international conferences and journals, which have been cited more than 5000 times. He is an editor of the IEEE Transactions on Wireless Communications (since 2014), IEEE Transactions on Vehicular Technology (since 2010) and received "Top Editor" award for outstanding contributions to the IEEE Transactions on Vehicular Technology in 2011, 2014 and 2015. He is a co-chair of IEEE Intelligent Transport Systems Society Technical Committee on Communication Networks. He has served as a chair, co-chair and TPC member in a large number of international conferences. He is a Fellow of IEEE and IET.

His research interest includes intelligent transport systems, applied graph theory and its applications in telecommunications, Internet of Things, wireless sensor networks, wireless localization techniques and network performance analysis.

Tao Han (M'13) received the bachelor's degree in information engineering, the master's degree in communication and information system, and the Ph.D. degree in information and communication engineering from the Huazhong University of Science and Technology (HUST), Wuhan, China, in 1990, 1993, and 2001, respectively. From 2010 to 2011, he was a Visiting Scholar with the University of Florida, Gainesville, FL, USA, as a Courtesy Associate Professor. He was a Visiting Professor with the University of Technology Sydney, Ultimo, NSW, Australia, in 2016. He has been an Associate Professor with the School of Electronic Information and Communications, HUST since 2001. He is also a Vice Chair of the China International Joint Research Center of Green Communications and Networking.

His research interests include wireless communications, multimedia communications, and computer networks. He is leading several projects funded by the National Natural Science Foundation of China, the Ministry of Science and Technology of China, and industries. He is currently serving as an Area Editor for the EAI Endorsed Transactions on Cognitive Communications. He was a recipient of the IET Networks Premium Awards in 2017 and the Best Paper Awards from the IEEE CIC ICCC 2017, the IEEE ISCIT 2016, and the IEEE GLOBECOM 2014.